Supporting Information

for

Parts-Per-Billion (ppb) Selective Iodine Sensors Leveraging Metal-Organic Framework Nanoenvironment

Arun S. Babal,[a,†] Samraj Mollick,[a,†] Waqas Kamal,[b] Steve Elston,[b] Alfonso A. Castrejón-Pita,[b] Stephen M. Morris,[b] and Jin-Chong Tan[a,]*

[a]Multifunctional Materials and Composites (MMC) Laboratory, Department of Engineering Science, University of Oxford, Parks Road, Oxford, OX1 3PJ, United Kingdom

[b]Department of Engineering Science University of Oxford, Parks Road, Oxford, OX1 3PJ, United Kingdom

[†]These authors contributed equally to this work.
[*]Corresponding email: jin-chong.tan@eng.ox.ac.uk

Contents

1. Materials preparation and characterization methods

1.1 Synthesis of MOF materials

Apart from F300 (purchased from Sigma Aldrich), the rest of the MOF materials employed in this study (ZIF-11, ZIF-65, ZIF-68, ZIF-70, ZIF-11, MOF-808) were synthesized by following the previously reported methods found in literature, with slight modifications.[1-5] All reagents and solvents were commercially available and used as received, sourced from Fisher Scientific, Alfa Aesar, and Fluorochem, depending on their availability.

ZIF-11: 2 mmol of benzimidazole was dissolved in 10 mL of ethanol and 8.5 mL of toluene, followed by the addition of ammonia hydroxide (2 mmol NH_3) under stirring at room temperature. After that, 1 mmol of zinc acetate dehydrate was added and stirred for the next 3 h at room temperature. The product of ZIF-11 was collected by centrifugation and washed with 50 mL of ethanol and dried at room temperature in the open air overnight.

ZIF-65: 0.5 mmol zinc acetate was soluble in 5 mL of DMF and rapidly mixed into 1 mmol of 2-nitroimidazole in 5 mL methanol under vigorous stirring. After 24 h of stirring at room temperature, the sample was centrifuged at 10,000 rpm to collect the product. The product was further washed three times with a copious amount of *N*, *N*-dimethylformamide (DMF) and methanol to remove the excess reactants and dried at 90 °C overnight.

ZIF-68: 0.5 mmol of 2-nitroimidazole, 0.16 mmol of benzimidazole and 0.5 mmol of $Zn(NO_3)_2 \cdot 6H_2O$ were mixed in 2 mL of different DMF solution separately. After that, three different solutions were combined and heated in a capped vial at 130 °C for 96 h and left to cool for 12 h. The mother liquor was decanted and the products were washed with excess DMF for four times.

ZIF-70: 0.36 mmol of 2-nitroimidazole, 0.36 mmol of imidazole and 0.36 mmol of $Zn(NO_3)_2 \cdot 6H_2O$ were mixed in 2 mL of different DMF solution separately. After that, three different solutions were combined and heated in a capped vial at 130 °C for 96 h and left to cool for 12 h. The mother liquor was decanted and the products were washed with excess DMF for four times.

ZIF-71: 2 mmol zinc acetate was soluble in 50 mL of methanol and rapidly mixed into a 50 mL methanol solution of 8 mmol of 4,5-dichloroimidazole under stirring. The mixed solution transformed from clean to turbid after a few seconds. After 24 hours of stirring at room

temperature, the sample was centrifuged at 10,000 rpm to collect the product. The product was further washed three times with a copious amount of methanol to remove the excess reactants.

MOF-808: Trimesic acid (210 mg, 1 mmol) and zirconyl chloride octahydrate (970 mg, 3 mmol) were dissolved in DMF/formic acid (30 mL/30 mL) and placed in a large screw-capped glass jar, which was heated to 130 °C for two days. A white precipitate of MOF-808 was collected by filtration and washed four times with 400 mL of fresh DMF. The DMF-washed compound was then immersed in 100 mL of acetone for four days and during this time the acetone was replaced two times per day to facilitate the solvent exchange process. The acetone-exchanged sample was then evacuated at room temperature for 24 h and at 150 °C for 24 h to yield an activated sample.

1.2 IDE sensor preparation

The prefabricated thin-film gold IDEs on a glass substrate were purchased from Micrux (ED-IDE3-Au), each sensor chip contains 184 pairs of gold microelectrode with a width and a gap size of 5 μm, respectively. Before sample deposition, the IDE electrodes were rinsed with isopropanol (HPLC grade, Sigma-Aldrich, ≥99.9%) and then dried under the nitrogen gas. The impedance value of empty IDEs was measured beforehand to perform a qualitative comparison between the sensitivity of different MOF samples. In the case of ZIF-70 MOF, for drop-casting and inkjet printing, the synthesized crystals were first broken into fine particles using a tip sonicator and then deposited on the IDE electrode.

Drop-cast method: As described in supplementary §1.1, the MOF materials were synthesized and left in the solvent suspension to avoid aggregation. The MOF suspension was pipetted out and drop casted on the active area of the IDE in such a way that on average ~1 mg of material was deposited for each of the MOF samples. Afterwards, the IDE was dried under ambient conditions. The amount of the deposited MOF was monitored using a high-resolution balance.

Single crystal: To prepare a single crystal prototype sensor, the cleaned IDE is placed inside the reaction vial of ZIF-70 MOF. The MOF synthesis reaction parameters were kept the same as described in §1.1. After the completion of the reaction, the IDE electrode was gently washed in the methanol solvent to avoid any stress-related cracking and then dried at room temperature. The IDE electrode was weighed before and after the crystal growth step to keep track of the

amount of deposited ZIF-70 amount, which was later used to quantify the adsorbed iodine amount.

Inkjet printing: The MOF 'ink', comprising an isopropyl alcohol (IPA) suspension of fine MOF particles without any additives, were printed using a commercially available printing system (Jetlab-II, MicroFab Technologies Inc.) which can deposit droplets within ±5 μm accuracy. To print MOF droplets without any satellite droplet, piezoelectric nozzle with an 80-μm orifice diameter was employed. The dispenser was plugged with a pneumatic pressure control system to control the back pressure so as to reduce the isopropanol solvent evaporation at the tip of the nozzle (the fast evaporation at the tip could lead to nozzle blockage). Figure S1 shows the dynamic shadowgraph images of the smooth MOF droplet formation process. The in-flight diameter of the falling droplet is ~50 μm. The IDE patterned substrate (Micrux interdigitated electrodes) was placed onto the bed of the printer. During printing, the substrate and printhead were maintained at room temperature of 21 °C. A rectangular array of droplets, according to the area of the IDE electrodes, were printed at a droplet spacing of 20 μm. Iodine sensing MOF based devices with a range of film thicknesses were produced by changing the print pass of the printhead.

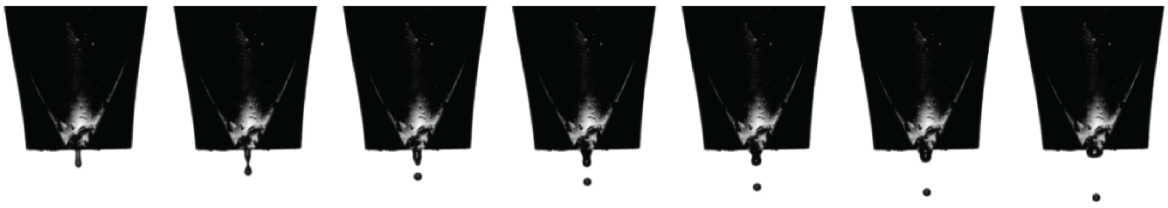

Figure S1: High-speed photography images of the printing process of an exemplar ZIF-70 MOF solution. The size of the nozzle orifice is 80 μm. The time interval between two adjacent frames is 48 μs.

Iodine Exposure

For iodine experiments, the MOF deposited IDE electrode and an excess of 50 mg of dry iodine was placed inside a 500 mL glass bottle. The sealed glass bottle was then placed inside an oven at 70 °C for 30 mins and later cooled down to room temperature. For each MOF,

three IDEs were prepared to ensure the repeatability of data. MOF sample with the highest iodine sensitivity was chosen to further carry out cyclic adsorption and desorption measurement for 3 cycles to confirm its reversibility. To do so, the sample was heated at 70 °C overnight.

1.3 Electrical response

The electrical response from the IDE sensor was recorded at room temperature at 35% RH (relative humidity) using the HIOKI IM3536 LCR meter in the frequency range of 4 Hz to 8 MHz at 1 V. To measure the sensitivity of the sample IDE at any point in time, the impedance, capacitance and phase angle parameters were obtained in parallel as a function of frequency. For in-situ experiments, a 467.6 ppb and 8.35, 16.7, 25.05, 33.40 ppm level I_2 environment was maintained by placing meshed iodine inside an in-house closed chamber alongside the sample IDE to simulate the real-time application. Subsequently, the impedance measurements were continuously collected at 10 Hz (1 V) as well as over the frequency range of 4 Hz to 8 MHz.

1.4 X-ray diffraction (XRD)

The powder XRD pattern for the different MOF samples was determined using the Rigaku MiniFlex benchtop X-ray diffractometer at a scan rate of 0.2°/min with a step size of 0.05°. Before the data collection, the MOF samples were pre-evacuated in a vacuum chamber at 100 °C overnight to minimize solvent effect.

1.5 Fourier-transform infrared (FTIR) spectroscopy

The FTIR spectra for the MOF samples were recorded using the Nicolet-iS10 FTIR spectrometer equipped with an attenuated total reflectance (ATR) sample accessory in the mid-IR region (650–4000 cm^{-1}) at a spectral resolution of 0.5 cm^{-1} after collecting the background spectrum using the identical parameters. The impact of iodine adsorption and desorption on infrared vibrational modes of MOF at room temperature as well as with time-dependent heating effect was studied by ATR-FTIR.

1.6 Raman spectroscopy

The Raman spectra were collected using the Bruker MultiRAM Raman spectrometer with sample compartment D418, equipped with a Nd-YAG-Laser (1064 nm) and a LN-Ge diode as a detector. The laser power used for sample excitation was 50 mW, and 64 scans were accumulated at a resolution of 1 cm^{-1}.

1.7 Thermogravimetric analyses (TGA)

The thermal stability of the MOF specimens was measured using the TGA-Q50 (TA Instruments) equipped with an induction heater (max temperature 1000 °C) and platinum sample holder under an N_2 inert atmosphere. The samples were heated at a rate of 10 °C/min from 30 to 800 °C.

1.8 UV−Visible diffuse reflectance spectroscopy (DRS)

The absorption spectra for samples were obtained using the 2600 UV−Vis spectrophotometer (Shimadzu) in the wavelength range of 200-1400 nm, equipped with an integrating sphere. The diffused reflectance spectra (DRS) were measured and converted using the Kubelka−Munk (KM) transformation to estimate the optical band gaps.

1.9 Optical microscopy and surface profilometry

Alicona profilometer was used to measure the surface texture such as the thickness of the deposited MOF layer. The surface topography was characterized by the infinite focus microscopy technique (Alicona Infinite Focus 3D profilometer) using the 5× optics on the profilometer.

2. Powder X-ray diffraction (PXRD) of different MOFs

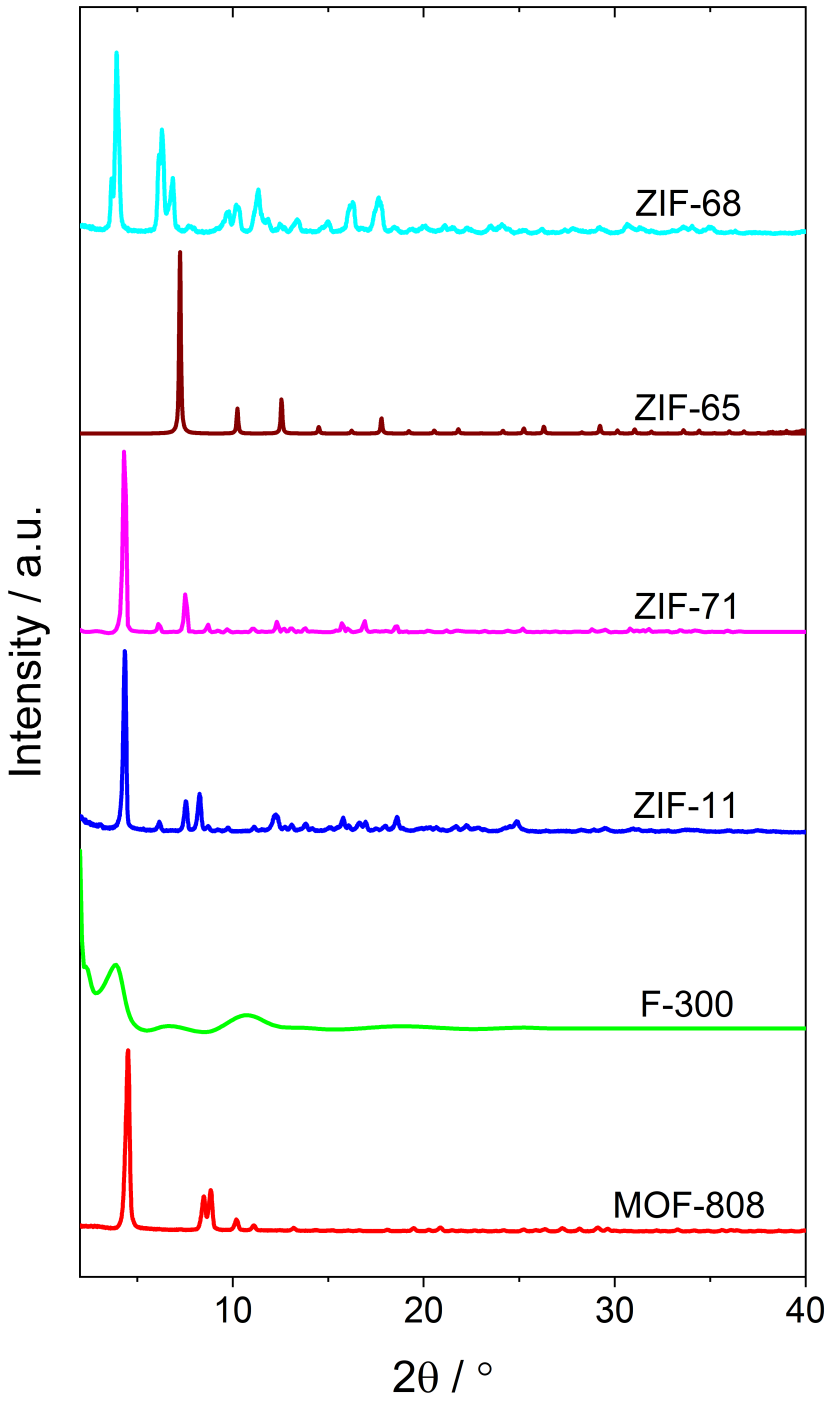

Figure S2: Normalized PXRD patterns of activated MOF powder samples.

3. IDE sensors integrating different MOF samples

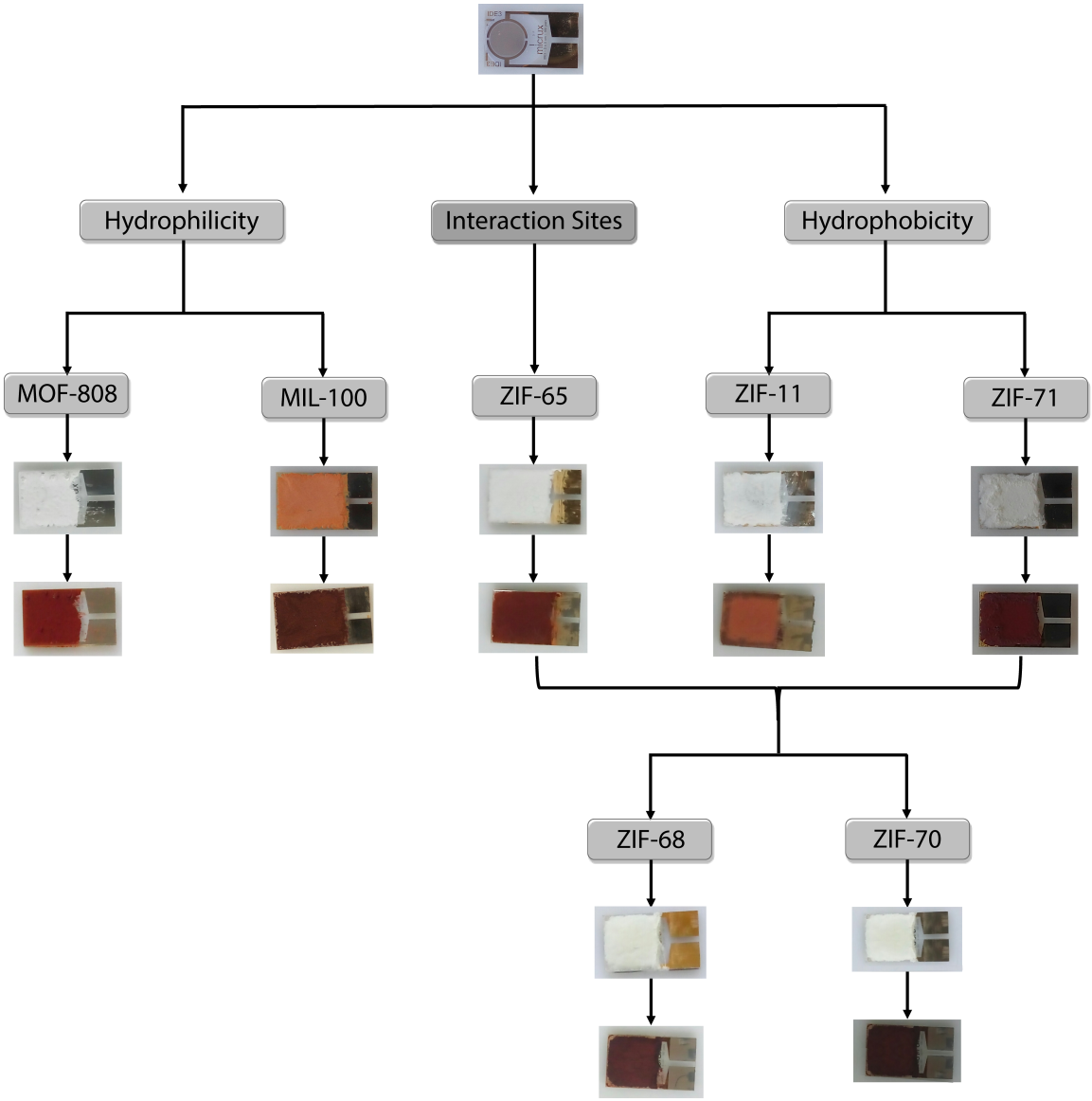

Figure S3: Photographs of prototype MOF@IDE sensors, before and after iodine exposure tests (top vs. bottom images of each MOF sample).

Table S1: Iodine adsorption dependent percentage change in the MOF weight.

MOF	Mass Change / %
MOF-808	50.0±12.0
F300	48.2±2.0
ZIF-11	10.7±4.8
ZIF-71	26.6±6.0
ZIF-65	47.0±1.2
ZIF-68	26.8±7.0
ZIF-70	91.0±8.2

4. MOF@IDE sensor response

4.1 Hydrophilicity effect of MOF-808 and F300

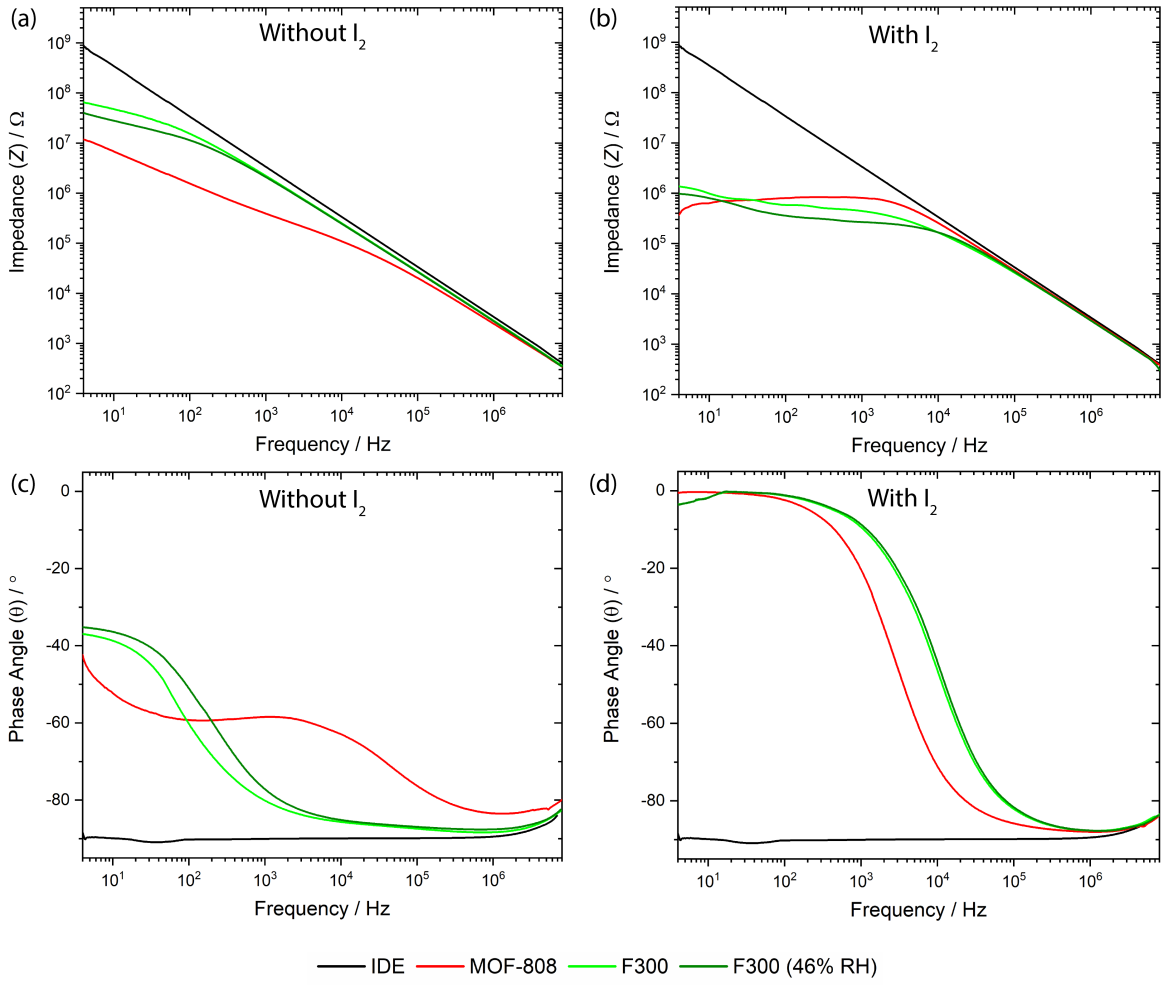

Figure S4: Effect of hydrophilicity on sensor impedance and phase angle: (a), (c) before and (b), (d) after iodine adsorption, respectively.

4.2 Hydrophobicity effect of ZIF-11 and ZIF-71

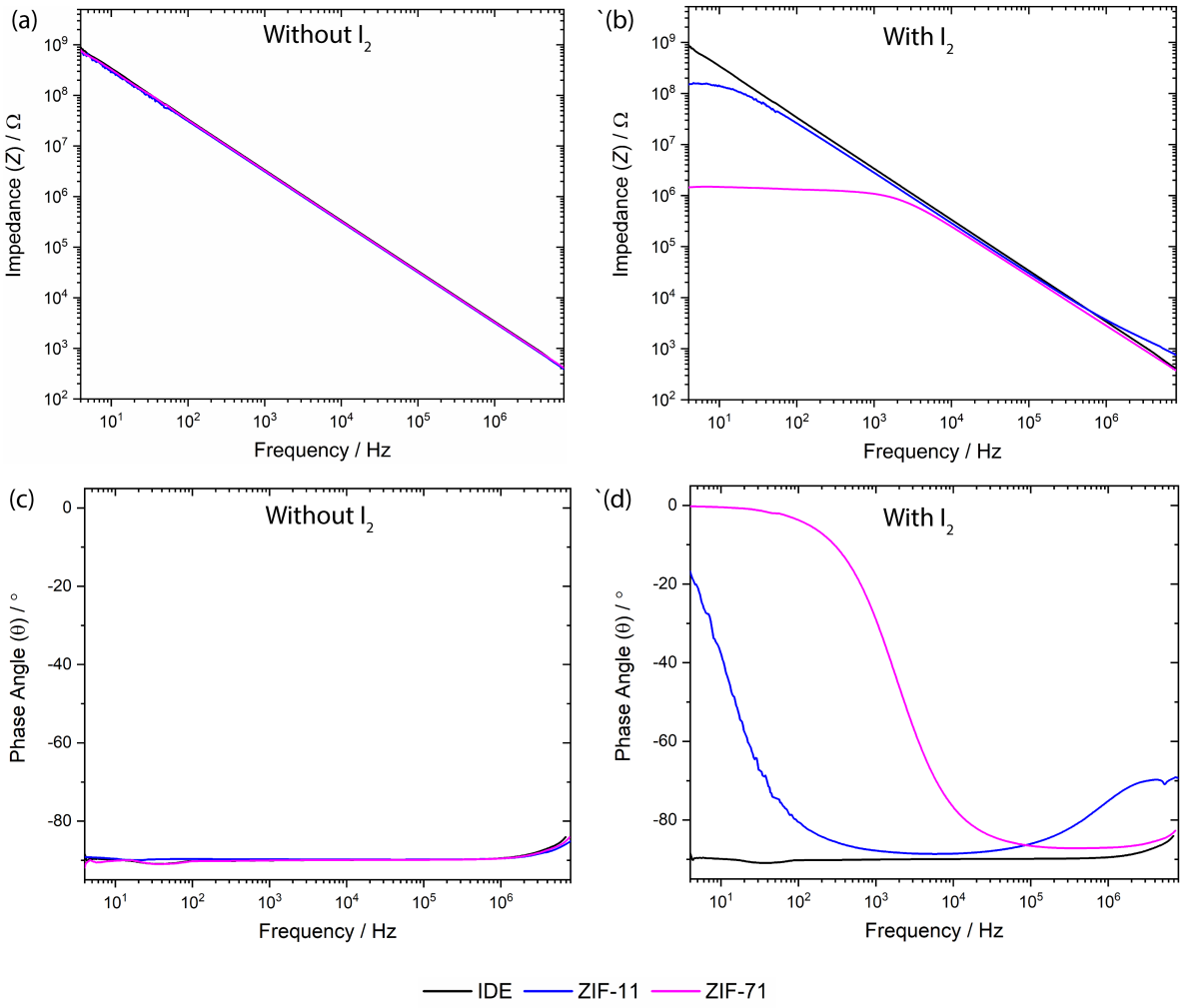

Figure S5: Hydrophobicity dependent alterations in sensor impedance and phase angle: (a), (c) before and (b), (d) after iodine adsorption, respectively.

4.3 Interaction sites effect of ZIF-65

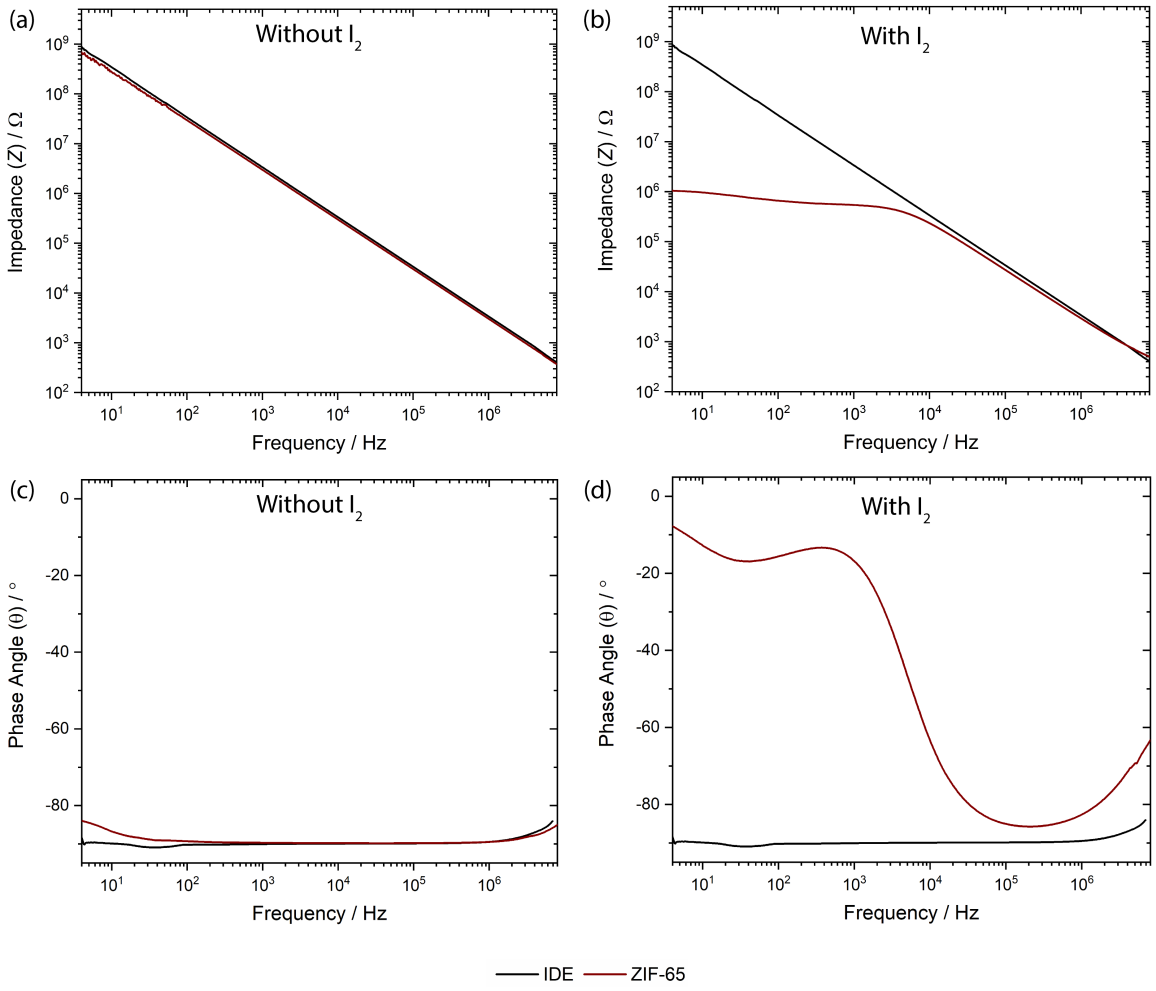

Figure S6: Interaction site dependent shift in sensor impedance and phase angle: (a), (c) before and (b), (d) after iodine adsorption, respectively.

4.4 Interaction sites with optimal hydrophobicity effects of ZIF-65 and ZIF-70

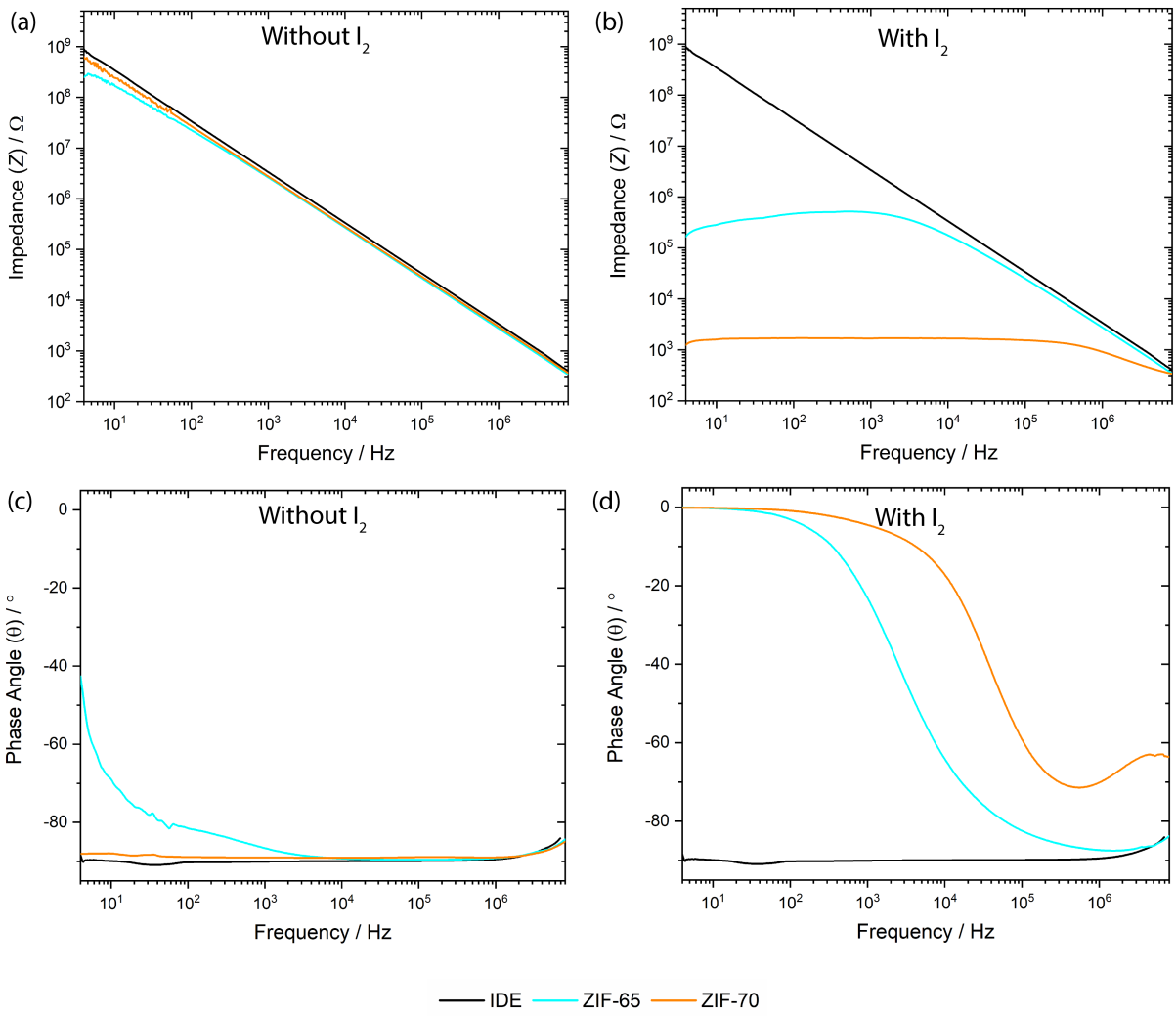

Figure S7: Combined effect of interaction site and hydrophilicity-hydrophobicity on sensor impedance and phase angle: (a), (c) before and (b), (d) after iodine adsorption, respectively.

5. Change in MOF@IDE response

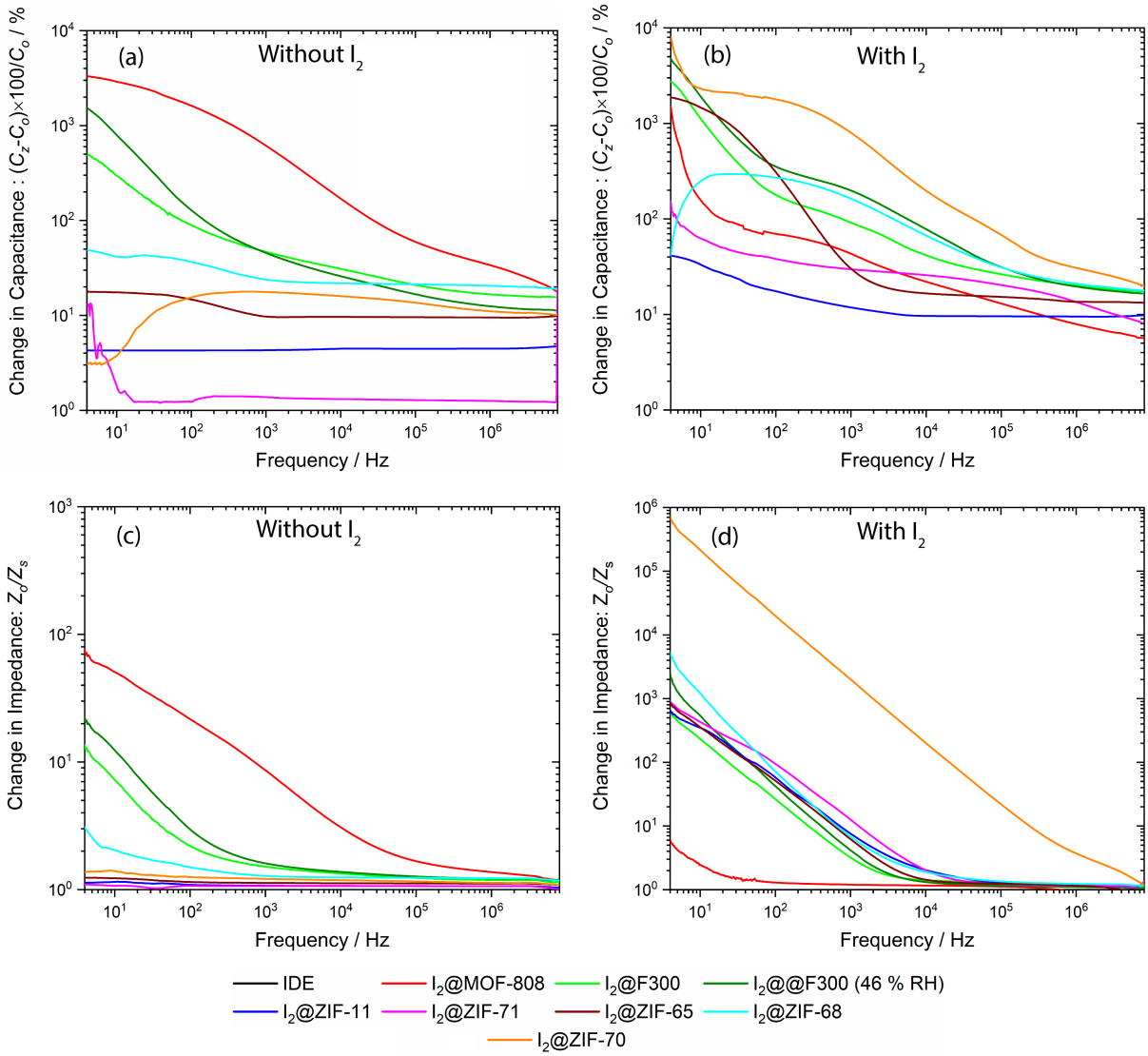

Figure S8: Variations in the electrical response of different MOF@IDEs: before and after iodine adsorption. (a), (b) Changes in capacitance and (c), (d) in impedance, as a function of frequency.

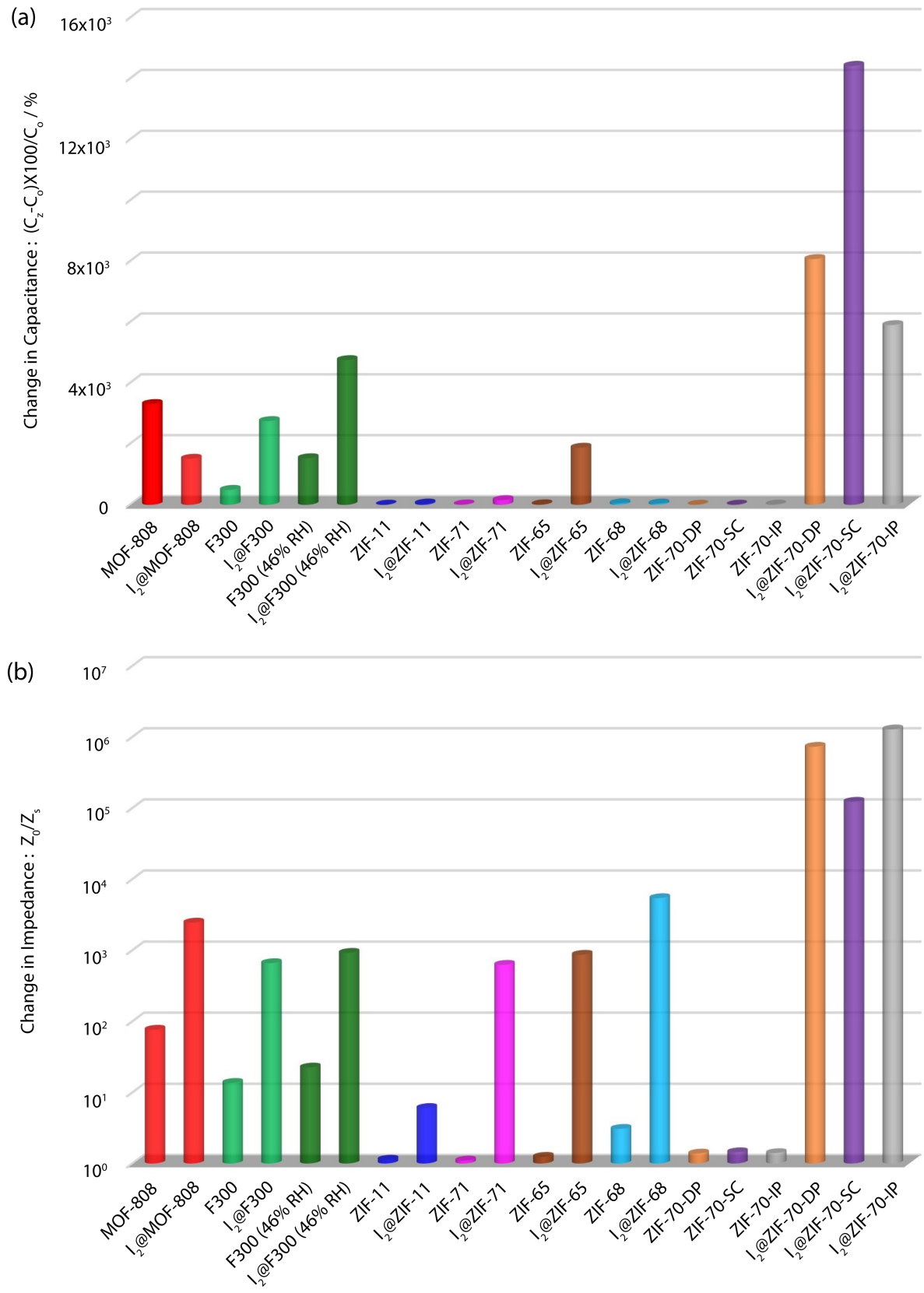

Figure S9: Comparative plots of the change in MOF@IDE output parameters determined at 4 Hz: (a) Percentage change in capacitance, and (b) ratio of sample impedance relative to an 'empty' IDE (no MOF). Note: DP = drop casting, SC = single-crystal and IP = inkjet printing.

Table S2: Enhancement in capacitance and impedance ratio of different drop-casted MOF@IDEs, before and after the I_2 exposure.

MOF Name	*n*-Fold in Enhancement	
	Capacitance $(C_z\text{-}C_o) \times 100/C_o$	**Impedance** Z_o/Z_s
MOF-808	3,311.1	76.1
I_2@MOF-808	1,512.8	2,439.2
F300	489.6	13.6
I_2@F300	2,751.2	656.3
F300 (46% RH)	1,530.5	22.4
I_2@F300 (46% RH)	4,754.9	916.8
ZIF-11	4.3	1.1
I_2@ZIF-11	41.4	6.0
ZIF-71	13.0	1.1
I_2@ZIF-71	153.5	622.3
ZIF-65	17.8	1.2
I_2@ZIF-65	1,876.3	862.2
ZIF-68	48.9	3.1
I_2@ZIF-68	41.3	5,394.3
ZIF-70	3.0	1.4
ZIF-70-SC	4.2	1.4
ZIF-70-IP	6.6	1.4
I_2@ZIF-70	8,074.6	725,042.7
I_2@ZIF-70-SC	14,422.2	122,347.9
I_2@ZIF-70-IP	5,904.5	1,275,056.9

6. Guest-dependent MOF@IDE response

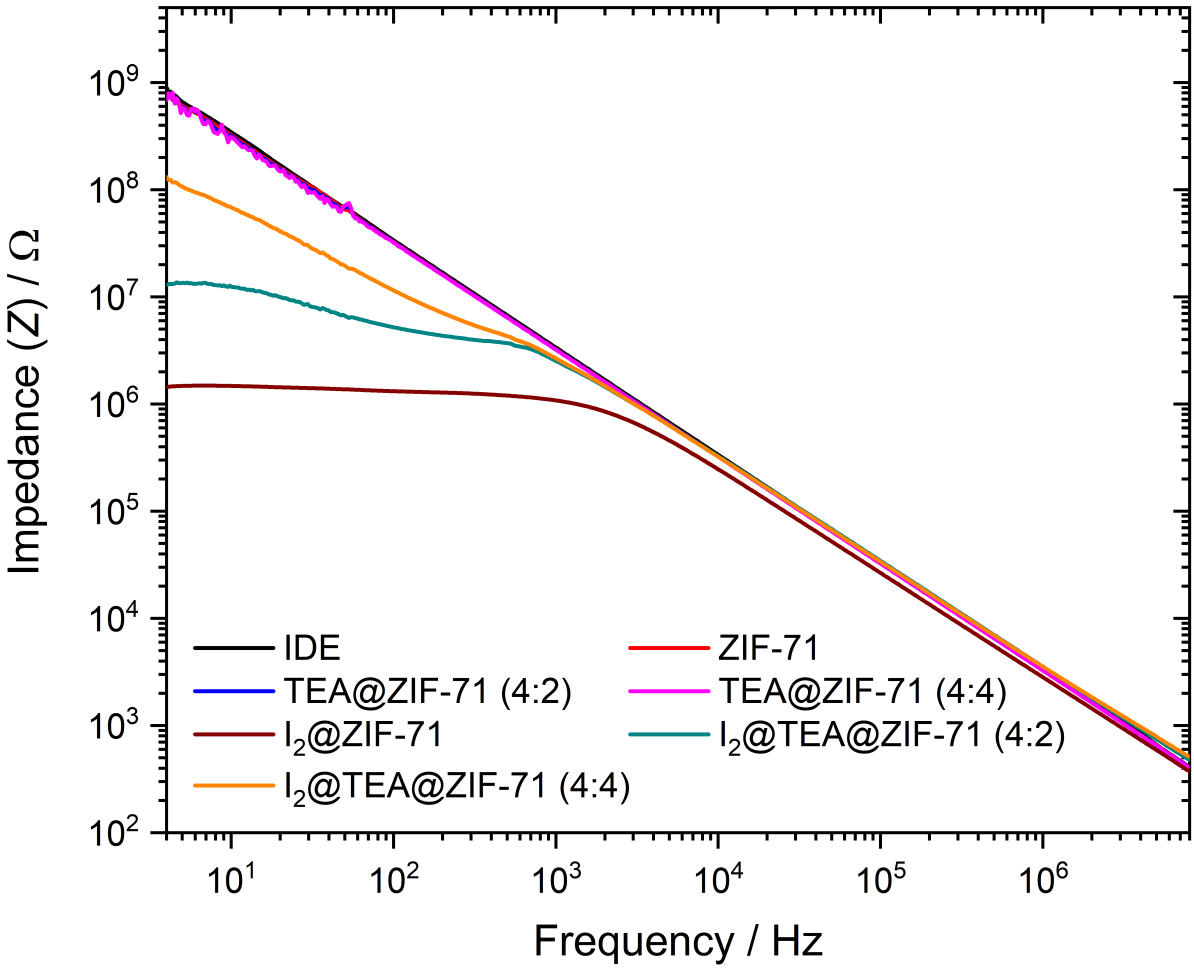

Figure S10: Effect of different amount of guest encapsulation in ZIF-71 framework on iodine sensing. The ratio of linker to TEA was varied during the ZIF-71 synthesis and expressed in label as ZIF-71(L: G), where L and G are the molar concentrations of the MOF linker and triethylamine (TEA) guest, respectively.

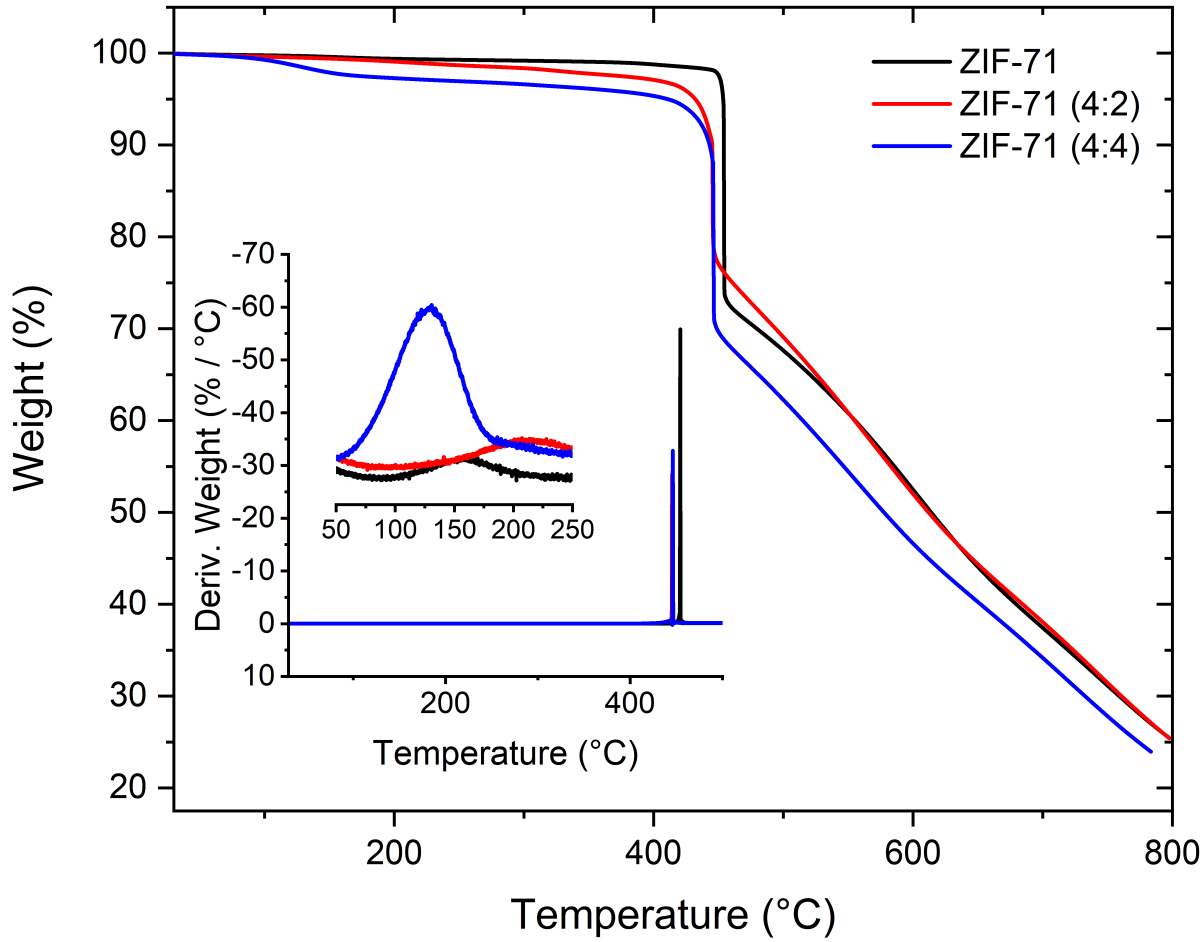

Figure S11: TGA analysis to show the presence of triethylamine (TEA) guest in ZIF-71 pores. The ratio of linker to TEA was varied during the ZIF-71 synthesis and expressed in label as ZIF-71(L: G), where L is linker and G is TEA Guest.

7. MOF@IDE sensitivity in the presence of different solvent vapors

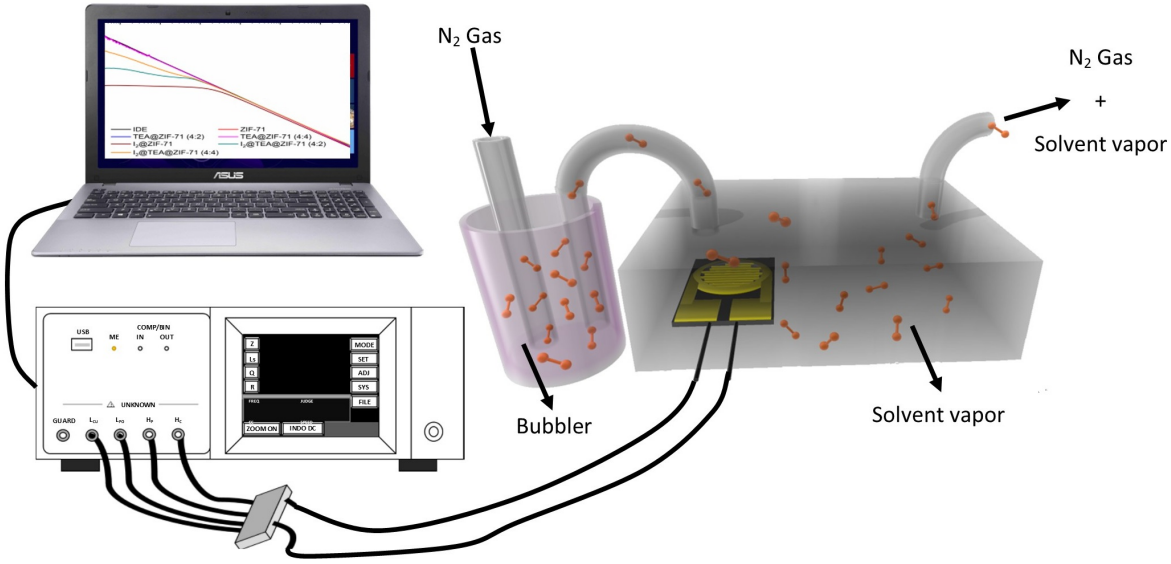

Figure S12: Customized setup designed for in-situ testing of various saturated vapour effects on the electrical impedance (*via* LCR meter) of the ZIF-70 MOF.

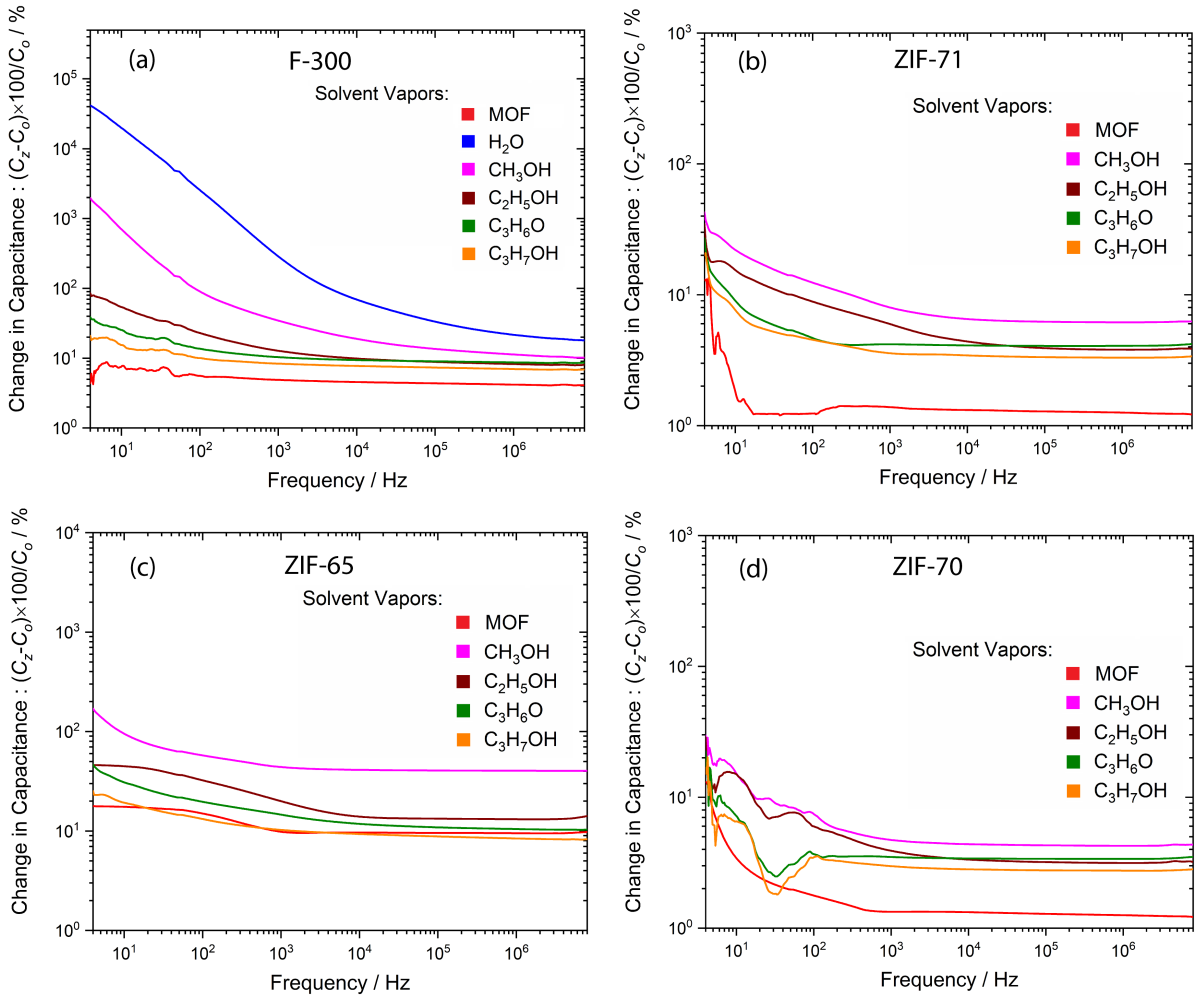

Figure S13: Solvent vapor dependent change in capacitance response for different MOF prototype sensors: (a) F300, (b) ZIF-71, (c) ZIF-65 and ZIF-70 MOFs.

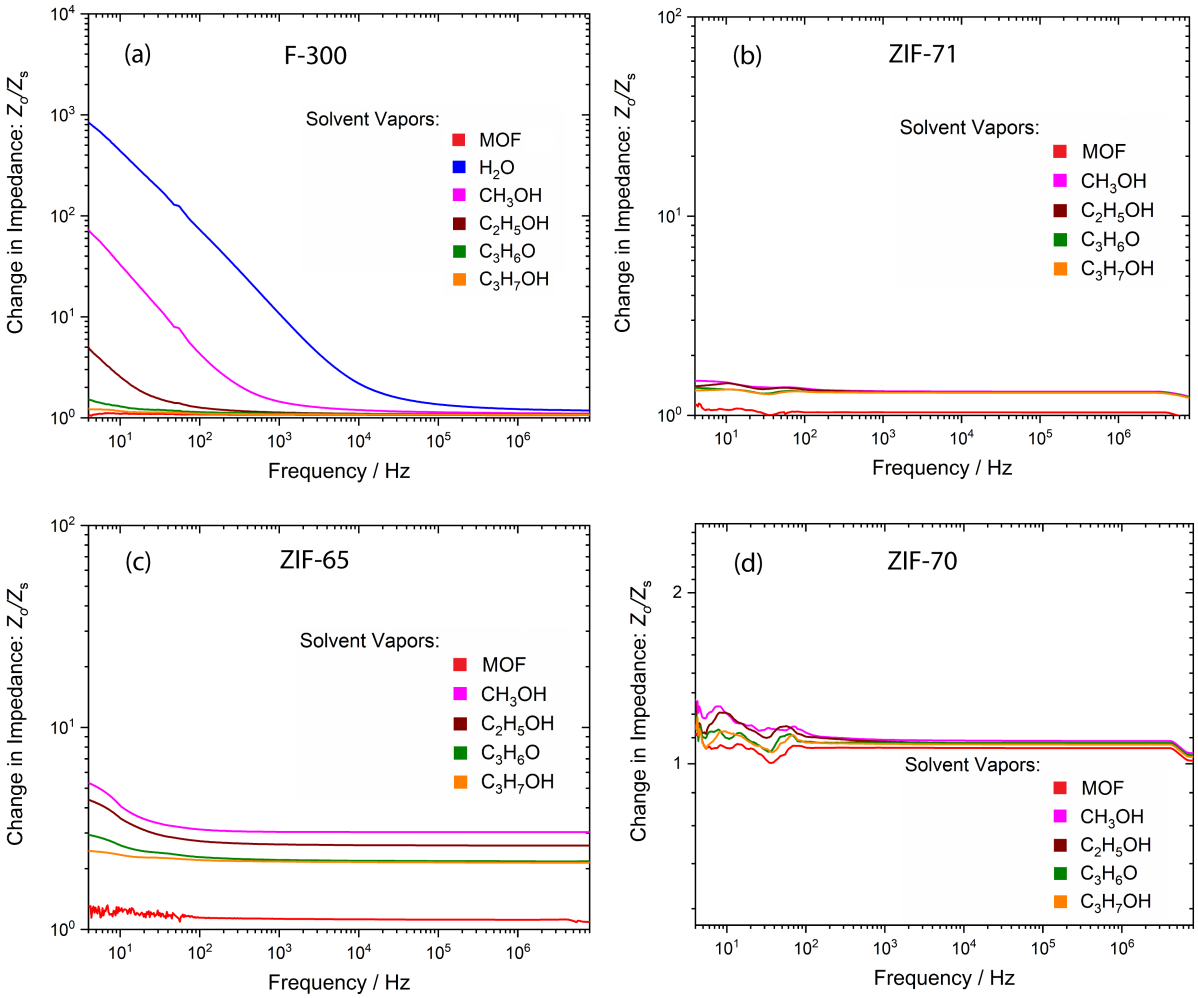

Figure S14: Solvent vapor dependent change in impedance response for different MOF prototype sensors: (a) F300, (b) ZIF-71, (c) ZIF-65 and ZIF-70 MOFs.

Table S3: A comparison between I_2 and various solvent-dependent changes in the impedance ratio of drop-casted ZIF-70 MOF.

Target Molecules@ZIF-70	**Change in Impedance (Z_0/Z_s)**
I_2@ZIF-70	725,042.7
Methanol	1.3
Ethanol	1.3
Acetone	1.2
Isopropanol	1.2

8. Adsorption-desorption response of ZIF-70 in the presence of solvent vapors

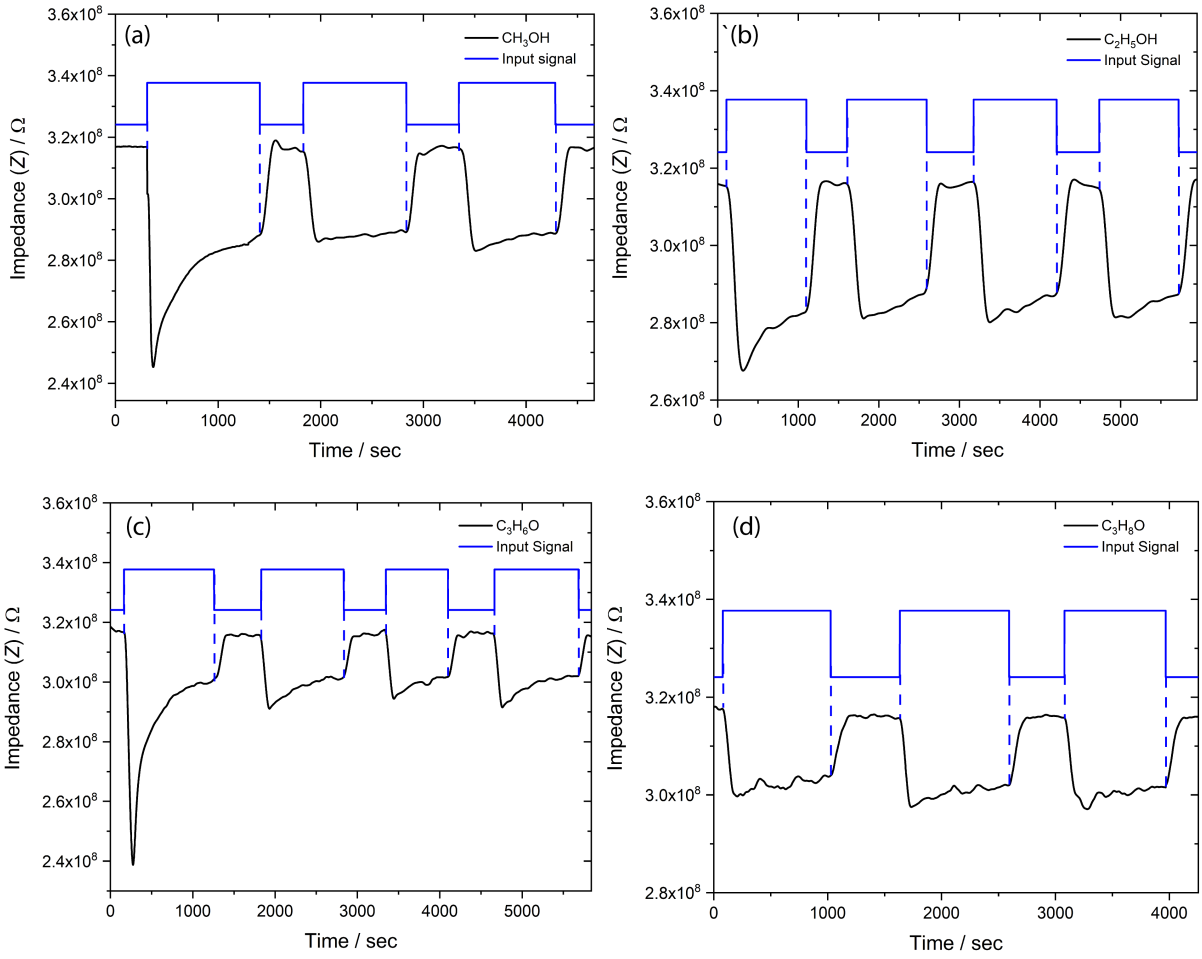

Figure S15: Solvent adsorption-desorption dependent cyclic impedance response for ZIF-70 MOF at 10 Hz, when exposed to (a) methanol, (b) ethanol, (c) acetone, and (d) isopropanol.

9. Single-crystal ZIF-70 MOF@IDE sensitivity in the presence of iodine

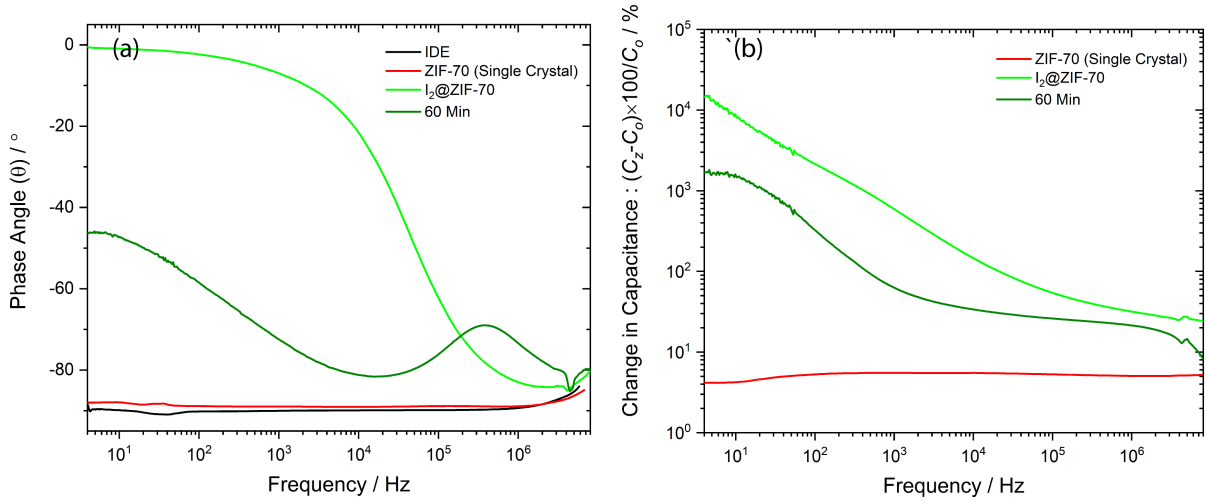

Figure S16: Variations of (a) phase angle and (b) capacitance in single-crystal ZIF-70 prototype sensor, before and after the iodine exposure.

10. Inkjet-printed ZIF-70 sample layer thickness by optical profilometry

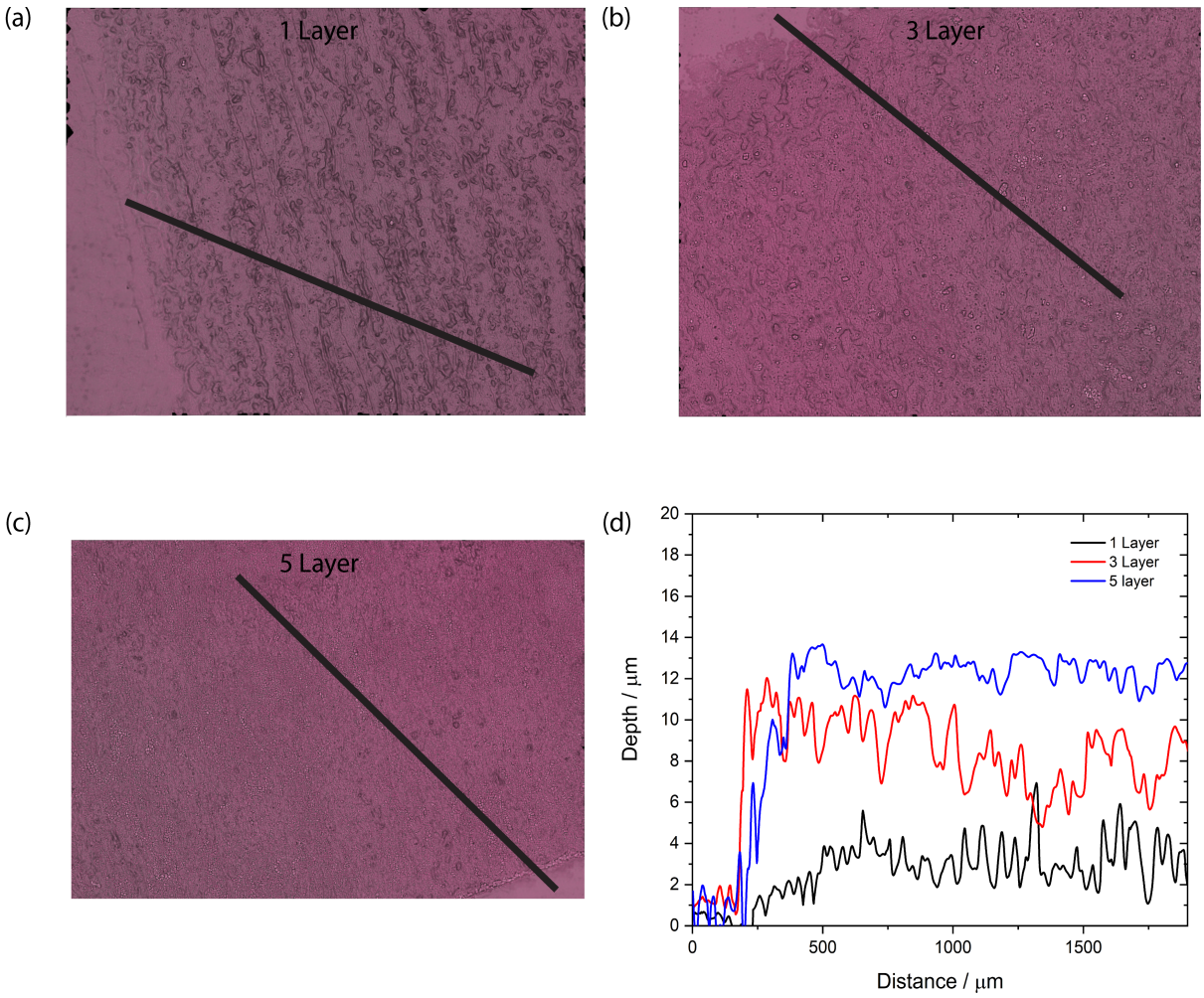

Figure S17: Optical images of inkjet-printed ZIF-70 layers: (a) 1 layer, (b) 3 layers and (c) 5 layers. (d) Plots of ZIF-70-layer height with respect to the distance associated with the black line marked in the corresponding optical images.

11. Inkjet-printed ZIF-70 MOF@IDE sensitivity in ppm and ppb levels

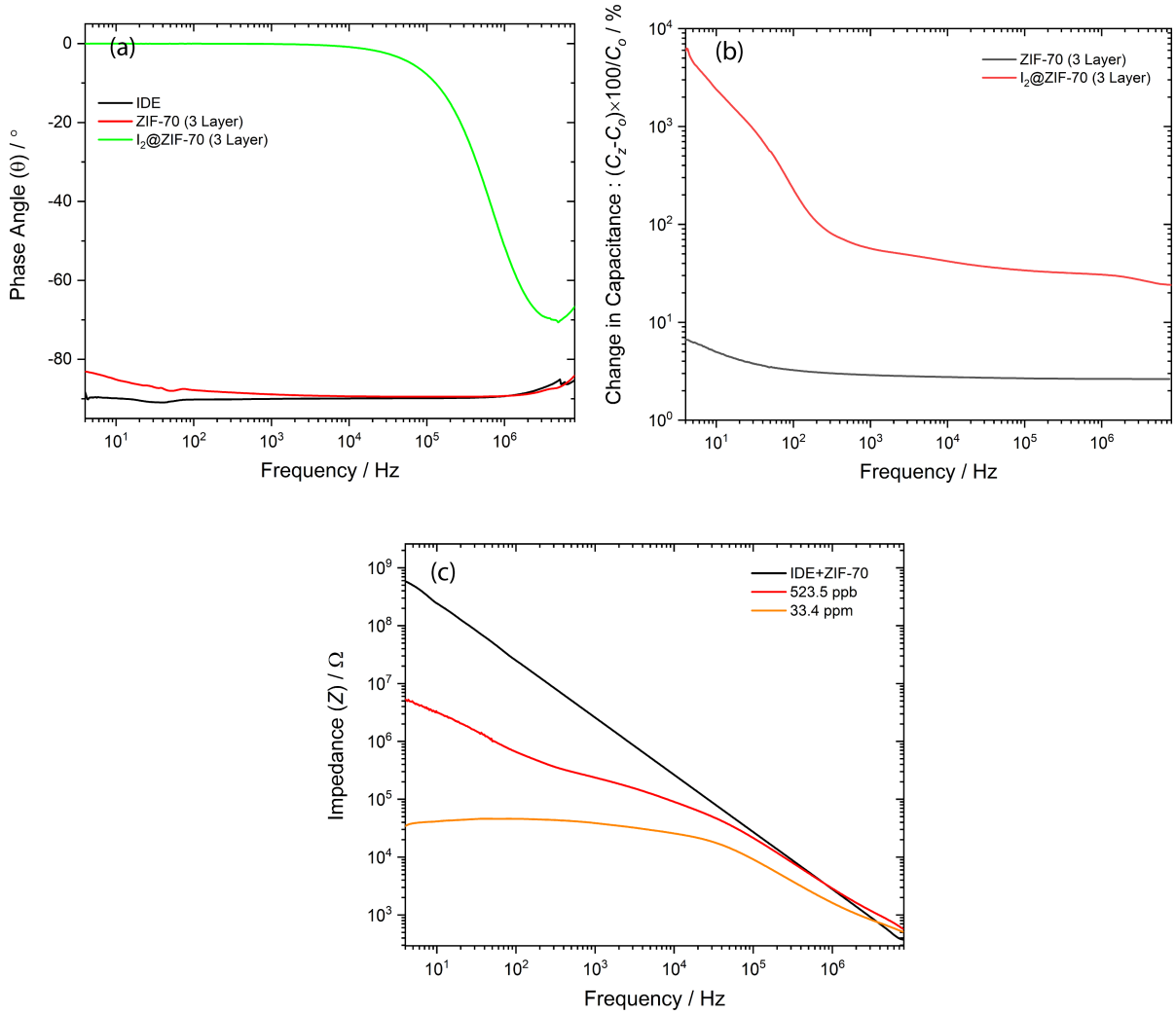

Figure S18: (a) Phase angle and (b) change in capacitance of 3-layer-ZIF-70@IDE, before and after iodine exposure. (c) Impedance sensitivity of 3-layer-ZIF-70@IDE prototype sensor performance at ppm and ppb concentration levels.

12. Characterization of ZIF-70 before and after I_2 uptake

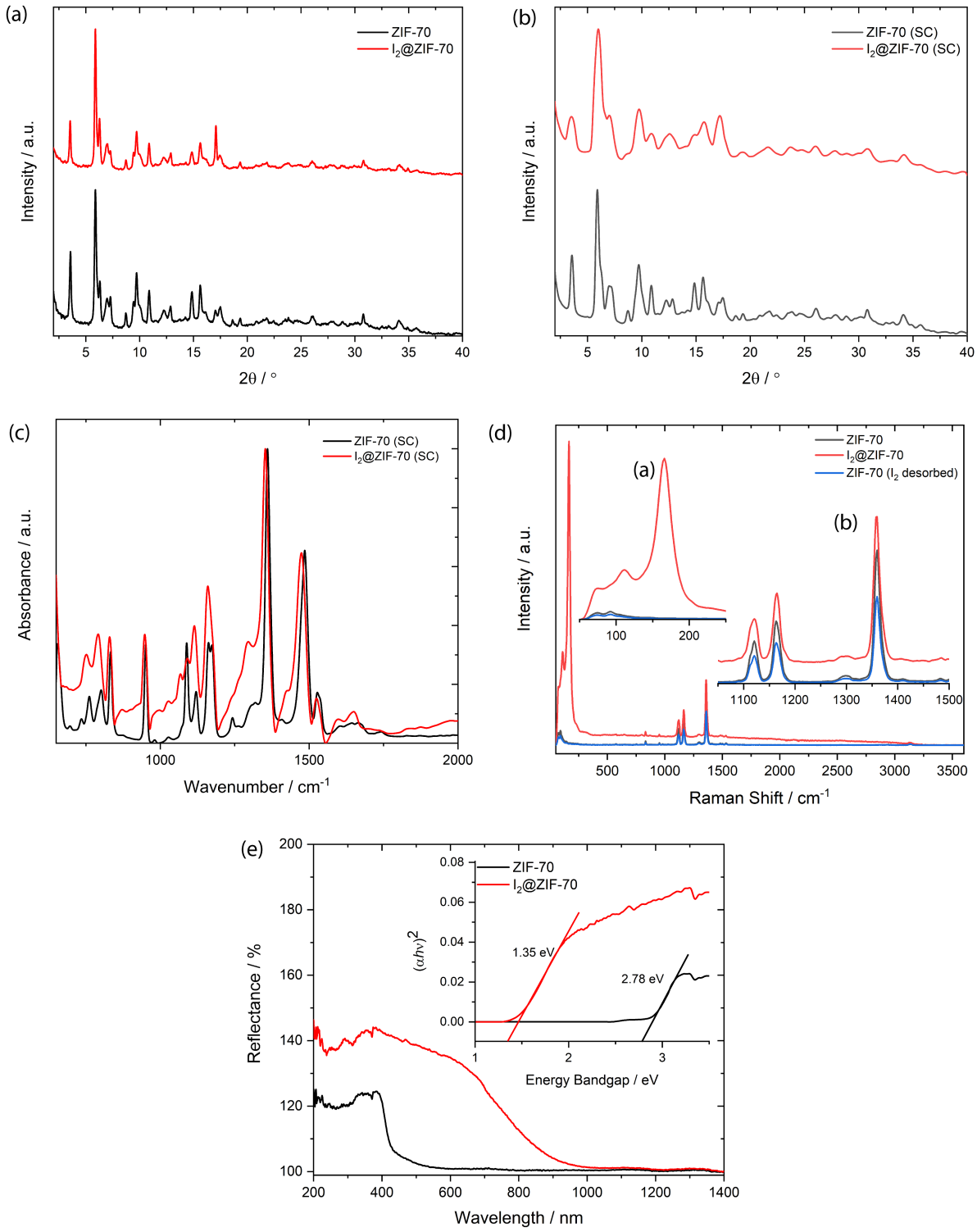

Figure S19: Material characterization of ZIF-70 MOF, before and after iodine exposure: XRD patterns of (a) powder and (b) single crystal of ZIF-70. (c) FTIR spectrum of ZIF-70 single crystal, and (d) Raman spectra of ZIF-70 powder. (e) UV-Vis diffuse reflectance spectra (DRS) with an inset of band-gap determination *via* Kubelka-Munk (KM) method.

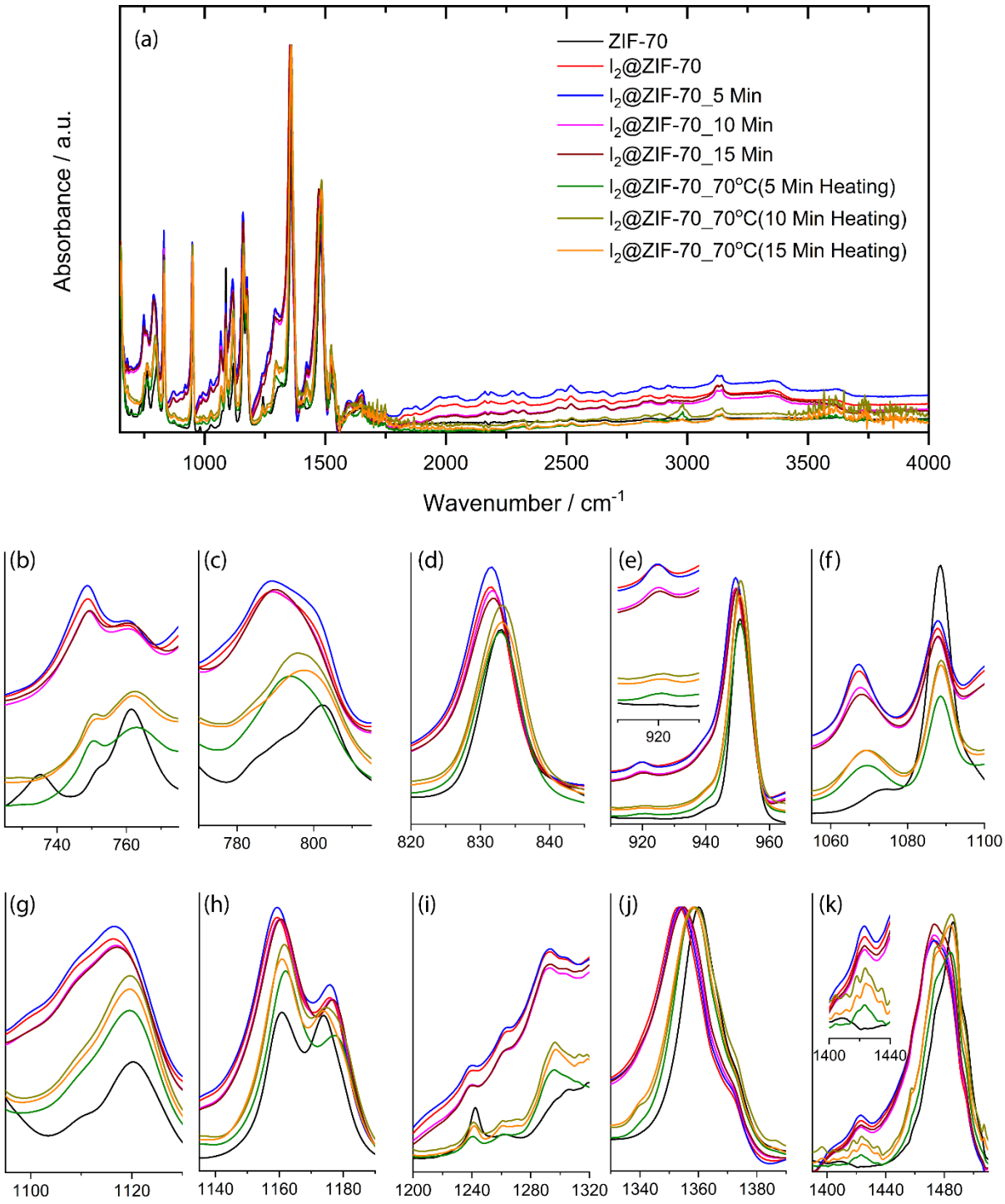

Figure S20: Time- and temperature-dependent iodine desorption analysis for ZIF-70 MOF using the FTIR spectra.

13. Sensor performance data

Table S4: Enhancement in the impedance ratio of the ZIF-70@sensor prepared using drop-casting, single crystal, and inkjet printing methods. The impedance measurements were performed under the DC and AC frequencies.

Method	DC	AC
Drop-casted	9.1×10^8	7.2×10^5
Single crystal	5.9×10^8	1.2×10^5
Inkjet printing	2.8×10^9	1.3×10^6

Table S5: Comparison of the sensor sensitivity between this work and other related investigations on IDE-based iodine sensors. Literature values were extracted from the published studies cited below.

Materials	Direct Current (DC)	Alternative Current (AC)	Reference
ZIF-70	2.84×10^9	54,973	This work
MFM-300 (Al)	< 1,000,000	< 10	*ACS Appl. Mater. Interfaces* **11**, 27982-27988 (2019).
ZIF-8	< 100,000	< 100	*ACS Appl. Mater. Interfaces* **9**, 44649-44655 (2017).
Polyacetylenic film	< 1,000	-	Sens. Actuators B **129**, 171 (2008).
Ag-mordenite	< 300	< 5	*Microporous Mesoporous Mater.* **280**, 82−87 (2019)

14. References

[1] M. He et al., Dalton Trans. 42 (2013) 16608.

[2] R. Banerjee et al., Science 319 (2008) 939.

[3] R. Banerjee et al., J. Am. Chem. Soc. 131 (2009) 3875.

[4] Y. Zhang et al., ACS Appl. Mater. Interfaces 12 (2020) 37477.

[5] E. Aunan et al., Chem. Mat. 33 (2021) 1471.